IJST EXPLORE International Journal of Science and Technology
CENTRE OF PROFESSIONAL RESEARCH PUBLICATIONS
ISSN 2049-7318

International Journal of Science and Technology Volume 3 No. 11, November, 2014

The electrochemical characteristics of an ultra–fine grain γ'-Ni_3Al coating in 3.5% NaCl solution

Onyeachu B.I, Oguzie E.E, Njoku D.I, Ukaga I
Electrochemistry and Materials Science Research Laboratory Department of Chemistry, Federal University of Technology Owerri, PMB 1526, Owerri, Nigeria

ABSTRACT

The study of the electrochemical characteristics of an ultrafine–grain γ'–Ni_3Al coating was undertaken, after exposure for 72 h in 3.5% NaCl solution, using open circuit potential, electrochemical impedance spectroscopy and potentiodynamic polarization techniques. The ultrafine–grain γ'–Ni_3Al was fabricated by annealing an electrodeposition of a Ni–Al composite coating at 600 ^oC for 1 h. Compared with an arc–melted γ'–Ni_3Al alloy; the ultrafine–grain γ'–Ni_3Al exhibited more positive corrosion potential with lower corrosion current density. This was attributed to the highly refined microstructure of the ultrafine–grain γ'–Ni_3Al which promoted a lower transient time for the formation an Al_2O_3– enriched corrosion product layer.

Keywords: *Grain refinement, γ'–Ni_3Al, EIS, Al_2O_3, corrosion resistance*

1. INTRODUCTION

One of the most effective means of improving the general material characteristics of many metals and alloys is by refining their surface microstructure; such as reducing the grain sizes down to the micron or submicron sizes to form ultrafine–grain (UFG) metals and alloys. The UFG metals and alloys usually possess better strength because of the abundance of grain boundary atoms and triple junctions [1]. Understanding how such surface modification can influence the chemical stability of these metals and alloys would go a long way to determine their technological application. The corrosion resistance of many metals and alloys has been greatly increased in wet corrosion environments through grain size reduction [2–5] because the UFG materials provide abundance of nucleation sites and high particle–particle proximity for the effective formation of a highly continuous, adherent and protective corrosion product layer, compared with their polycrystalline coarse grain counterparts.

The conventional γ'–Ni_3Al intermetallic is well–known for its high melting point, low density and is an excellent candidate for high temperature application due to its ability to form a mature Al_2O_3 scale [6–10]. Compared with the coarse grain counterpart, UFG γ'–Ni_3Al possesses higher resistance to oxidation and better scaling mechanism in dry corrosion environments at high temperature because of a lower transient time for the formation of the protective and highly adherent Al_2O_3 [10, 11]. Electrodeposition of Ni–Al composites followed by subsequent heat treatment in vacuum leads to the formation of the UFG γ'–Ni_3Al as coatings on desired metal substrates [10]. The content and distribution of the Al particles in the Ni–Al composite and the annealing treatments like temperature and time are important factors which control the phase transformation of the pure Ni grains and Al particles into the γ'–Ni_3Al phase [11]. UFG γ'–Ni_3Al coating was obtained after annealing a Ni–Al composite with 20 vol. % of Al particles at 825 ^oC for 3 h [10], and a Ni–28wt. %Al composite at 600 ^oC for 2 h [11].

In a wet corrosion environment, it is envisaged that the electrochemical corrosion of the γ'–Ni_3Al could be improved through such grain size refinement, provided a lower transient time for the enrichment of the corrosion product layer with Al_2O_3 can be guaranteed in aqueous solutions. Unfortunately, such studies have not been given adequate attention. In the present work, we electrodeposited a Ni–37wt.%Al composite on Ni substrate, and subjected it to vacuum annealing treatment at 600 ^oC for 1 h. Thereafter we employed electrochemical methods to characterize the corrosion behaviour of the resultant UFG γ'–Ni_3Al after 72 h exposure in 3.5% NaCl solution, compared with a pure arc–melted γ'–Ni_3Al alloy fabricated by arc melting. We hope that the study will encourage the application of UFG γ'–Ni_3Al as coating for low temperature applications.

2. EXPERIMENTAL

2.1. Materials Preparation

The γ'–Ni_3Al alloy coupons had dimensions 12 X 10 X 2 mm^3. The coupons were grinded to a final 800 grit size with SiC paper, washed with distilled water and ultrasonically cleaned in acetone. Electrodeposition of the Ni–Al composite was performed at 2 A/dm^2 from a Ni–sulphate bath containing 150 g/L $NiSO_4.6H_2O$, 0.1 g/L Sodium Dodecyl Sulphate, 15 g/L NH_4Cl, 15 g/L H_3BO_3 and loaded with 300 g/L of 1µm size Al particles. Electrodeposition was performed at 30 ^oC for 2 h, using a reciprocating perforated plastic as agitator at 200 rpm speed. During the electrodeposition, the cathodes were pure Ni coupons with dimension 12 X 10 X 2 mm^3. The average Al content in the Ni–Al composite was 37wt.%, according to EDAX surface analysis. The annealing treatment of the Ni–Al composite was performed under a pressure of 10^{-5} Pa at 600 ^oC for 1 h. The phase characterization of the arc–melted γ'–Ni_3Al alloy and Ni–37wt.%Al composite before and after annealing treatment was performed using XRD.

2.2. Electrochemical measurements

The electrochemical measurements were carried out using PARSTAT 273A Potentiostat/Galvanostat (Princeton Applied Research). The UFG and arc–melted γ'–Ni_3Al samples (used as working electrodes) were prepared by embedding in a mixture of paraffin and rosin, exposing a working area of 1 cm^2 for corrosion tests. Saturated calomel electrode (SCE), which was connected through a Luggin capillary, was employed as reference electrode while a platinum sheet was used as counter electrode. The electrochemical measurements were performed after 72 h of exposure in 3.5% NaCl solution to ensure the formation of a corrosion product layer on the surfaces of the samples. The γ'–Ni_3Al samples were subjected to open circuit potential, E_{ocp}, measurement by measuring the variation of potential with time until a stable E_{ocp} value was attained. Electrochemical impedance spectroscopy was performed at E_{ocp} using a signal recovery model 5210 lock–in amplifier attached to the potentiostat in a frequency range of 100 kHz to 0.01 Hz with a signal amplitude perturbation of 10 mV. Potentiodynamic polarization test was performed in the potential range from –0.25 V/E_{ocp} to +0.25 V/SCE at a scan rate of 0.166 mV/s.

3. RESULTS AND DISCUSSION

3.1. Characterization of ultrafine–grain γ'–Ni_3Al

The cross sections of the Ni–Al composite before and after the annealing treatment are provided in Figure 1. In Figure 1(a), the Al particles (the dark dots) could be seen very well dispersed throughout the electrodeposited Ni matrix in the composite coating. About 20% by weight of Al particles existed in the cross–section of the as–deposited composite coating, as the corresponding EDAX elemental analysis showed in Figure 1(b). The SEM cross–section of the composite coating, after annealing at 600 ^oC for 1 h, is provided in Figure 1(c), with its corresponding EDAX analysis in Figure 1(d). Obviously, the annealing treatment caused the coarsening of the Al particles. Several micro–pores could also be seen in the cross–section of the as–annealed composite. This can be more clearly seen in the SEM magnified cross–section morphology of the as–annealed composite after 1 h at 600 ^oC, Figure 2(a), and is attributed to the Al particles consumption based on the elemental mapping in Figure 2(b). The XRD patterns for the electrodeposited Ni–Al composite before and after the annealing treatment are provided in Figure 3(a) and 3(b), respectively. The result showed that the annealing, at 600 ^oC for 1 h caused the Ni grains and Al particles to react and form the γ'–Ni_3Al phase. For comparison, the XRD pattern for the coarse grain γ'–Ni_3Al is provided in Figure 3(c).

3.2. Electrochemical Characterization

3.2.1. Open circuit potential measurement

After 72 h exposure in the 3.5% NaCl solution, the evolutions of the open–circuit potential with time for the arc–melted and UFG γ'–Ni_3Al sample are provided in Figure 4. The UFG γ'–Ni_3Al exhibited more positive E_{ocp} value than the arc–melted sample. The E_{ocp} value provides information about the active surface area of the metallic material exposed for the electrochemical reactions, and the susceptibility of the metallic material to dissolution [12]. Assuming the formation of a corrosion product layer, this implies that a more compact and inert corrosion product layer was formed on the surface of the UFG γ'–Ni_3Al which decreases its susceptibility to dissolution. Therefore, an abundance of nucleation sites is made available by the UFG γ'–Ni_3Al, during the 72 h exposure in 3.5% NaCl solution, whereby the formation of a highly continuous and stable corrosion product layer is greatly encouraged by an easy linkage of the corrosion product nuclei because of the highly reduced inter–particle spacing in the UFG γ'–Ni_3Al. Compared with the arc–melted sample, this phenomenon may also be attributed to the formation of a higher composition of the highly protective Al_2O_3 in the corrosion product formed by the UFG γ'–Ni_3Al after the 72 h immersion in the 3.5% NaCl solution.

3.2.2. Electrochemical impedance spectroscopy measurement

Electrochemical impedance spectroscopy can provide information about the rate and mechanism of the electrochemical reaction occurring at the γ'–Ni_3Al surface/electrolyte interface. After 72 h immersion in the 3.5% NaCl solution, the impedance results for the arc–melted and UFG γ'–Ni_3Al samples, obtained at E_{ocp}, are presented in the Nyquist (Figure 5 (a)) and Bode phase angle (Figure 5(b)) plots. Relative to the arc–melted sample, the UFG γ'-Ni_3Al displayed larger semicircle size in the Nyquist plot and higher phase angle maxima (especially at low frequency) in the Bode plot. These indicate greater corrosion resistance for the UFG γ'–Ni_3Al. The shapes of the Nyquist plots for both arc–melted and ultrafine–grain γ'–Ni_3Al show two capacitive loops; a slight loop at high frequency and another, more pronounced, loop at low frequency. These corresponded with two time constants in the phase angle plots, supporting the proposition that both the arc–melted and UFG γ'–Ni_3Al surfaces could form a corrosion product layer during this 72 h exposure. The first time constant at high frequency was attributed to the processes occurring at the corrosion product layer/electrolyte interface while the second time constant was attributed to the processes occurring beneath the corrosion product layer, i.e. at the substrate/electrolyte interface [12]. The equivalent circuit model in Figure 6 was, therefore, adapted as model for the impedance behaviour of the arc–melted and UFG γ'–Ni_3Al samples after modelling the impedance spectra with Zsimpwin software. The values of the corresponding circuit elements are given in Table 1.

Table 1: Impedance parameters for arc–melted and ultrafine–grain γ'-Ni_3Al after 72 h immersion in 3.5% NaCl solution

Sample	$R_s(\Omega\ cm^2)$	$Q_{cp}(10^{-5}\ F/cm^2)$	$R_{cp}(\Omega cm^2)$	$Q_{dl}(10^{-5}\ F/cm^2)$	$R_{ct}(10^4\ \Omega\ cm^2)$
Arc–melted γ'-Ni_3Al	3.001	2.6	470	0.53	0.49
UFG γ'-Ni_3Al	3.350	1.5	858	0.48	2.2

The electrolyte solution resistance is represented by R_s. The Q_{cp} and R_{cp}, respectively, represent the capacitance of the corrosion product layer and the resistance of its pores to penetration of the electrolyte solution beneath the layer. On the other hand, Q_{dl} and R_{ct}, respectively, represent the capacitance of charge in the double layer beneath the corrosion product layer and the resistance to charge transfer in this double layer. The Q values are indicators of the dielectric properties of the corrosion product layers. The Q values were generally lower for the UFG γ'-Ni_3Al than the arc–melted alloy. This implies a lower store of charge both in the corrosion product–electrolyte interface and the substrate–electrolyte interface, for the UFG γ'–Ni_3Al sample, and attests to the fact that its corrosion product layer was both compact and inert in the 3.5% NaCl solution. These low Q values corresponded with higher R_{ct} value for the UFG γ'–Ni_3Al. The R_{ct} value is a measure of the corrosion resistance of the samples. The value of capacitance, Q, is an indication of the thickness of the corrosion product formed [13]. Assuming no change occurs in the dielectric constant, the reciprocal of the capacitance (1/Q) is directly proportional to the thickness of the corrosion product layer. Thus, a denser and more compact layer was formed on the surface of the UFG γ'–Ni_3Al, compared with the porous layer formed on the arc–melting γ'-Ni_3Al, after 72 h exposure in 3.5% NaCl solution. Moreover, the increased compactness of the UFG γ'–Ni_3Al corrosion product may be linked with Al_2O_3 enrichment of its corrosion product/substrate interface. This is the reason for the clearly higher phase angle maximum at low frequency, compared with the arc–melted γ'–Ni_3Al alloy. This is the reason that the UFG γ'–Ni_3Al exhibited higher corrosion resistance after 72 h exposure in 3.5% NaCl solution, than the arc–melted γ'–Ni_3Al.

3.2.3. Potentiodynamic polarization measurement

The results from potentiodynamic polarization measurements can provide insight on how the grain size refinement can modify the cathodic and anodic half–reactions occurring when the γ'–Ni_3Al surface is exposed to the 3.5% NaCl solution. After the 72 h exposure, the polarization curves obtained for the arc–melted and UFG γ'–Ni_3Al samples in 3.5% NaCl solution are provided in Figure 7. Both samples did not exhibit any active–passive transition throughout the potential scan range. The UFG γ'–Ni_3Al displayed more positive corrosion potential, E_{ocp}, value and lower corrosion current density, i_{ocp}, as shown in Table 2.

Table 2: Polarization parameters for arc–melted and ultrafine–grain γ'-Ni_3Al after 72 h immersion in 3.5% NaCl solution

Sample	E_{ocp} (mV/SCE)	i_{ocp} (μA/cm^2)	β_a (mV/dec.)	β_c (mV/dec.)
Arc–melted γ'-Ni_3Al	–377	5.734	123	–271
UFG γ'-Ni_3Al	–290	4.098	208	–201

This implies a higher corrosion resistance for the UFG γ'–Ni_3Al sample, and supports the observation during the impedance measurement. During the polarization, the UFG γ'–Ni_3Al showed higher cathodic current density but lower current density during the anodic scan. The anodic current is related with the active dissolution of the surface grains of the γ'–Ni_3Al samples in the solution, whereas notable cathodic reactions may include the reduction of water molecules into hydroxide ions, in such neutral solution as 3.5% NaCl solution. The impedance result showed that both γ'–Ni_3Al samples could form corrosion product layers during the 72 h exposure in the 3.5% NaCl solution. As is well known, the electrochemical corrosion mechanism of many metallic materials usually commences with the surface adsorption of water molecules, (reaction (1), leading to the formation of corrosion product layers composed of a hydroxide–enriched outer layer, (reactions 2 & 3), and inner layer enriched with oxides through dehydration of the hydroxides, (reactions 4 & 5). The chemistry is provided in the reactions below.

1. $2H_2O_{(l)} + O_{2(g)} + 4e^- \longrightarrow 4OH^-_{(aq)}$
2. $Ni^{2+}_{(aq)} + 2OH^-_{(aq)} \longrightarrow Ni(OH)_{2\,(s)}$
3. $Al^{3+}_{aq)} + 3OH^-_{(aq)} \longrightarrow Al(OH)_{3\,(s)}$
4. $Ni(OH)_{2(s)} \longrightarrow NiO_{(s)} + H_2O_{(l)}$
5. $2Al(OH)_{3(s)} \longrightarrow Al_2O_{3(s)} + 3H_2O_{(l)}$

Unlike the arc–melted sample, the highly refined surface microstructure of the UFG γ'–Ni_3Al should, therefore, favour more rapid formation of this corrosion product layer and its subsequent thickening due to the reduced inter–particle spacing. This mechanism would promote the dehydration and allow the penetration of oxygen, rather than water, through the corrosion product layer where the formation and growth of the highly protective Al_2O_3 is triggered, as shown below. The Al_2O_3 has been reported to exhibit very low solubility and conductivity in aqueous solutions in the pH range of 4–9 [14]. The Al_2O_3 enrichment of the UFG γ'–Ni_3Al corrosion product layer is, therefore, the reason that the UFG γ'–Ni_3Al exhibited higher corrosion resistance than the arc–melted alloy. During the polarization after 72 h exposure in 3.5% NaCl solution, the Al_2O_3 enrichment immensely lowers the rate of dissolution of the surface grains in the UFG γ'–Ni_3Al during the anodic potential scan. It has been reported that the Al_2O_3 enrichment reduces the oxidation rate of UFG γ'–Ni_3Al by serving as a barrier to the supply of Ni atoms to the oxidation front [10]. The present result shows that such mechanism could be replicated at low temperature in wet corrosion environments. Nevertheless, the Al_2O_3 enrichment leads to an increase in cathodic current density during the polarization of the UFG γ'–Ni_3Al. It is plausible that cathodic half–reactions occur around the Al component of the γ'–Ni_3Al as well as around the formed Al_2O_3. Such could be possible through the acquiring of surface hydration by the Al_2O_3 during the formation of a most stable

polymorph. The chemistry of this Al_2O_3 formed by the UFG γ'–Ni_3Al is, therefore, the reason for the observed higher cathodic current density during the polarization (Figure 7). On the other hand, the Ni component of the γ'–Ni_3Al acts as the anode around which oxidation half–reaction occur. Thus when developed, the Al_2O_3 enrichment could promote the formation of a highly adherent NiO layer. Furthermore, the Al_2O_3 lowers the conductivity of the UFG γ'–Ni_3Al corrosion product layer towards the adsorption of electro–migrated chloride ions in the 3.5% NaCl solution. Chloride ions are well known to locally attack and penetrate corrosion product layers formed on metals and alloys during corrosion, exposing more active sites on the surfaces for active dissolution. In the case of the UFG γ'–Ni_3Al, the pitting should greatly be blocked when the pitting front meets a well–developed Al_2O_3 layer. In addition, the Al_2O_3 formation is sustained by the abundance of atoms in the grain boundaries of the UFG γ'–Ni_3Al. This is the reason that the UFG γ'–Ni_3Al exhibited greater corrosion resistance than the arc–melted γ'–Ni_3Al after 72 h immersion in 3.5% NaCl solution.

4. CONCLUSION

The electrochemical characteristics of an ultrafine–grain (UFG) γ'–Ni_3Al have been investigated after 72 h exposure in 3.5% NaCl solution. Compared with an arc–melted γ'–Ni_3Al alloy, the UFG γ'–Ni_3Al exhibited more positive corrosion potential and lower corrosion current density. The grain refinement modified the electrochemical characteristics of the γ'–Ni_3Al by increasing the rate of cathodic half–reactions but decreasing the anodic half–reactions. This was attributed to a higher composition of Al_2O_3 in the UFG γ'–Ni_3Al corrosion product layer.

Acknowledgements

Onyeachu B.I is grateful to TWAS, the World Academy of Science and the Chinese Academy of Science (CAS) for the award of a CAS-TWAS Postgraduate Fellowship.

REFERENCES

[1]. Wang S.G, Shen C.B, Long K, Yang H.Y, Wang F.H, Zhang Z.D (2005), Preparation and electro

[2]. Wang S.G, Shen C.B, Long K, Zhang T, Wang F.H, Zhang Z.D (2006), Preparation and electrochemical corrosion behavior of bulk nanocrystalline ingot iron in HCl acid solution，J. Phys. Chem. (B109) 2499 - 2503

[3]. Wang X.Y, Li D.Y (2002), Mechanical and electrochemical behavior of nanocrystalline surface of 304 stainless steel, ElectrochimicaActa (47) 3939 - 3947

[4]. Kwok C.T, Cheng F.T, Man H.C, Ding W.H (2006), "Corrosion Characteristics of Nanostructured Layer on 316L Stainless Steel Fabricated by Cavitation-annealing", J. Materials Letters (60) 2419-2422

[5]. Ye W, Li Y, Wang F.H (2006), Effects of nanocrystallization on the corrosion behavior of 309 stainless steel, J. ElectrochimicaActa (5) 4426 – 4432

[6]. Stoloff N.S, Liu C.T, Deevi S.C (2000), "Emerging applications of intermetallics", J. Intermetallics (8) 1313-1320

[7]. Lee D.B, Santella M.L (2004), High temperature oxidation of Ni3Al alloy containing Cr, Zr, Mo, and B, J. Material Science & Engineering (A374) 217–223.

[8]. Cao G.J, Geng L, Zheng Z.Z, Naka M (2007), "The oxidation of nanocrystalline Ni3Al fabricated by mechanical alloying and spark plasma sintering", J. Intermetallics (15) 1672-1677

[9]. Pérez P, González-Carraco J.L, Adeva P (1997), Oxidation behavior of a Ni_3Al PM alloy, J. Oxidation of Metals (48) 143–170.

[10]. Peng X, Li M, Wang F (2011), A novel ultrafine-grained Ni_3Al with increased cyclic oxidation resistance, J. Corrosion Science (53) 1616 – 1620

[11]. Zhou Y.B, Zhang H.J (2011), Effect of annealing treatment on cyclic-oxidation of electrodeposited Ni-Al nanocomposite, . Trans Nonferrous Metal Society China (21) 322 – 329

[12]. Harvey J.F, Schweinsberg D.P (2005), A guide to polarisation curve interpretation: deconstruction of experimental curves typical of the $Fe/H_2O/H^+/O_2$ corrosion system, J. Corrosion Science (47) 2125–2156

[13]. Ghoneim A.A, Mogoda A.S, Awad K.A, El-TaibHeakal (2012), Electrochemical Studies of Titanium and its Ti-6Al-4V Alloy in Phosphoric Acid Solutions, Int. J. Electrochem. Sci. (7) 6539 - 6554

[14]. Pourbaix M (1974) Atlas of electrochemical equilibria in aqueous solutions, NACE Cebelcor, Huston, 1974

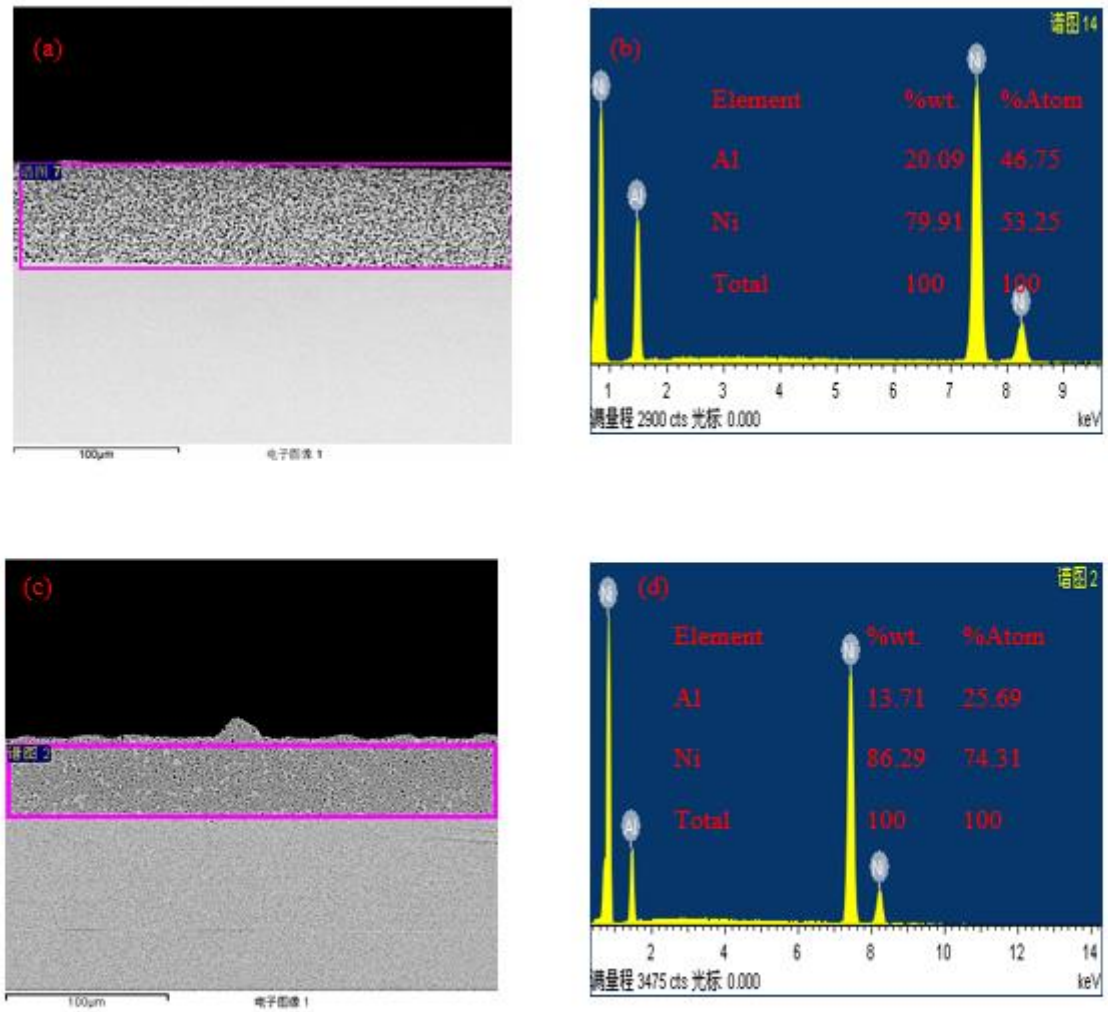

Figure 1: SEM cross–section morphologies with corresponding EDAX analysis for Ni–37Al composite (a, b) before annealing, (c, d) after 1 h annealing at 600 °C

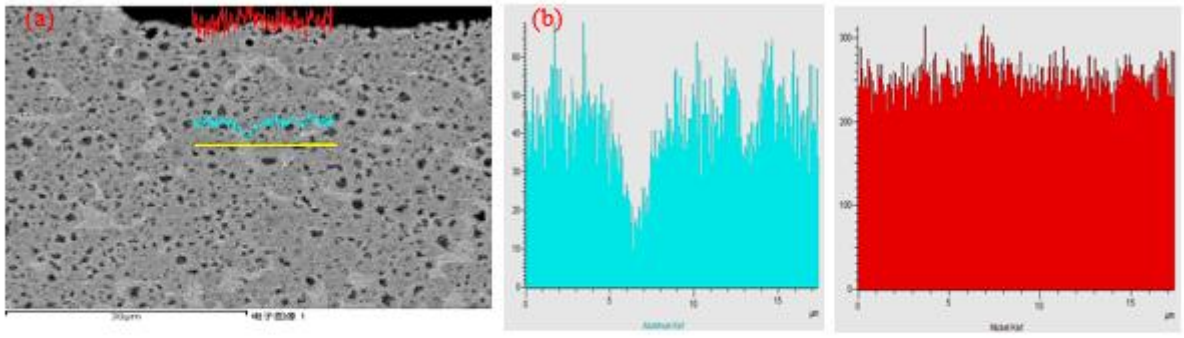

Figure 2: Magnified SEM morphology of the cross–section of Ni–37Al composite annealed for 1 h at 600 °C (a) with corresponding EDAX elemental mapping (b)

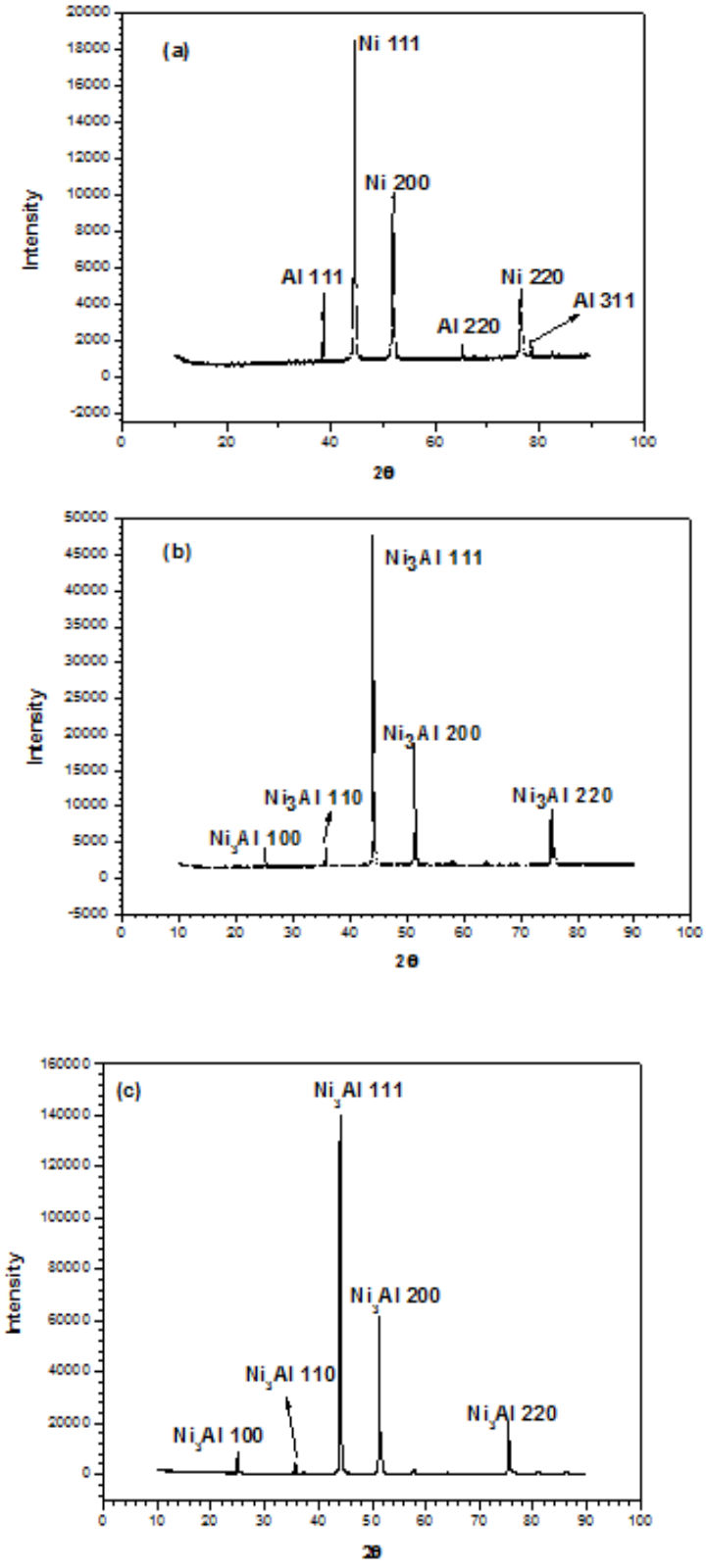

Figure 3: XRD patterns for electrodeposited Ni–37Al composite (a), Ni–37Al composite after 1 h annealing (b) and arc–melted γ'–Ni_3Al alloy (c).

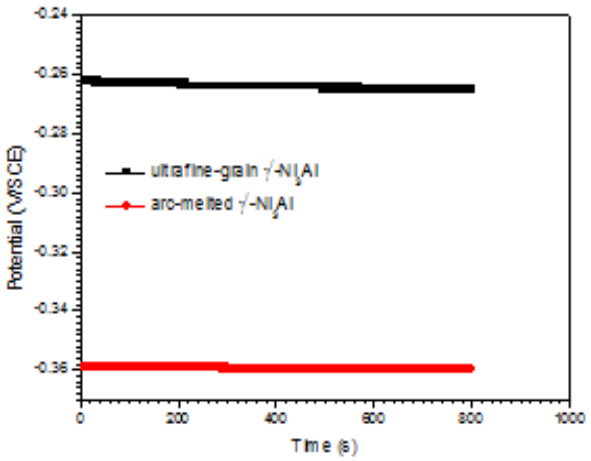

Figure 4: Variation of open circuit potential for arc–melted and ultrafine–grain γ'–Ni_3Al after 72 h immersion in 3.5% NaCl solution

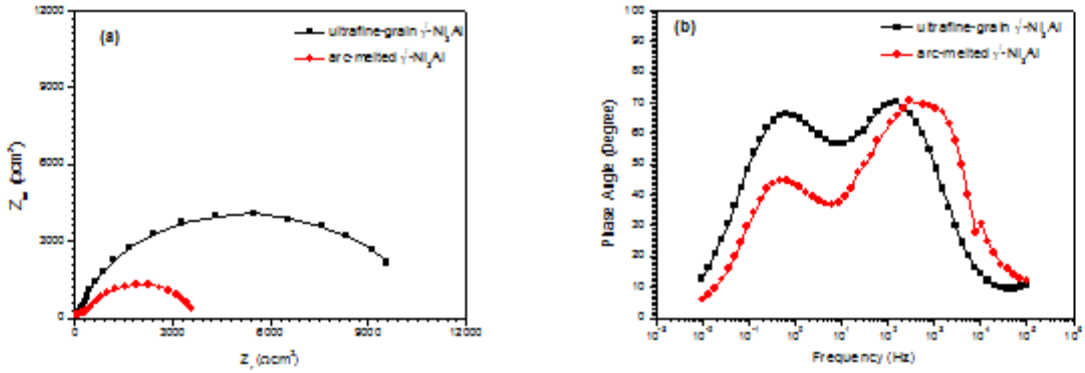

Figure 5: Impedance plots for arc–melted and ultrafine–grain γ'–Ni_3Al after 72 h immersion in 3.5% NaCl solution, shown in (a) nyquist and (b) BODE phase angle formats

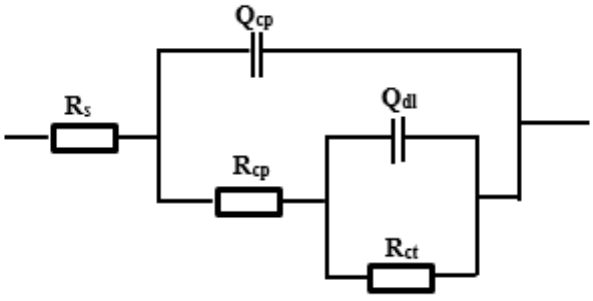

Figure 6: Equivalent circuit model for the impedance behaviour of arc–melted and ultrafine–grain γ'–Ni_3Al after 72 immersion in 3.5% NaCl solution

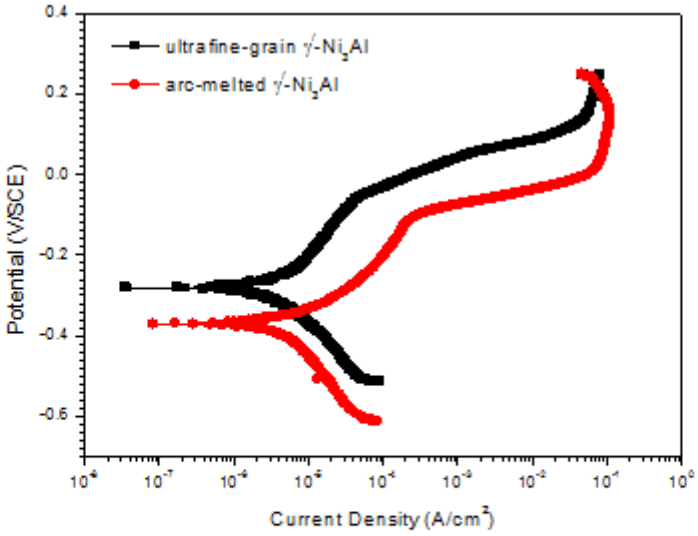

Figure 7: Potentiodynamic polarization plots for arc–melted and ultrafine–grain γ'–Ni_3Al after 72 h immersion in 3.5% NaCl solution